Title
Prefrontal-Subthalamic Hyperdirect Pathway Modulates Movement Inhibition in Humans

Journal
Neuron, 106(4)

ISSN
0896-6273

Authors
Chen, Witney
de Hemptinne, Coralie
Miller, Andrew M
et al.

Publication Date
2020-05-01

DOI
10.1016/j.neuron.2020.02.012

Peer reviewed

HHS Public Access

Author manuscript

Neuron. Author manuscript; available in PMC 2021 May 20.

Published in final edited form as:

Neuron. 2020 May 20; 106(4): 579–588.e3. doi:10.1016/j.neuron.2020.02.012.

Prefrontal-subthalamic hyperdirect pathway modulates movement inhibition in humans

Witney Chen[1,6,*], **Coralie de Hemptinne**[1], **Andrew M. Miller**[2], **Michael Leibbrand**[3], **Simon J. Little**[4], **Daniel A. Lim**[1,5], **Paul S. Larson**[1,5], **Philip A. Starr**[1,*]

[1]Department of Neurological Surgery, University of California San Francisco, San Francisco, CA 94143, USA [2]School of Medicine, University of Kansas, Kansas City, KS 66160, USA [3]Doculayer, Inc., Amsterdam, Noord-Holland, 1021 JL, The Netherlands [4]Department of Neurology, University of California San Francisco, San Francisco, CA 94143, USA [5]San Francisco Veterans Affairs Health Care System, San Francisco, CA 94121, USA [6]Lead Contact

SUMMARY

The ability to dynamically change motor outputs, such as stopping an initiated response, is an important aspect of human behavior. A hyperdirect pathway between the inferior frontal gyrus and subthalamic nucleus is hypothesized to mediate movement inhibition, but there is limited evidence for this in humans. We recorded high spatial and temporal resolution field potentials from both the inferior frontal gyrus and subthalamic nucleus in 21 subjects. Cortical potentials evoked by subthalamic stimulation revealed short latency events indicative of monosynaptic connectivity between the inferior frontal gyrus and ventral subthalamic nucleus. During a stop signal task, stopping-related potentials in the cortex preceded stopping-related activity in the subthalamic nucleus, and synchronization between these task-evoked potentials predicted the stop signal reaction time. Thus, we show that a prefrontal-subthalamic hyperdirect pathway is present in humans and mediates rapid stopping. These findings may inform therapies to treat disorders featuring perturbed movement inhibition.

eTOC BLURB

Chen et al. identify a fast, non-stop pathway between the prefrontal cortex and subthalamic nucleus in humans, using multisite invasive brain recordings. This pathway is critically involved in the stopping of ongoing actions. Modulation of this pathway may be a means to treat disorders of inhibitory control, such as impulsivity.

[*]Corresponding Authors: Witney Chen: witney.chen@ucsf.edu, Philip A. Starr: philip.starr@ucsf.edu.

AUTHOR CONTRIBUTIONS

W.C. and P.A.S. conceived the research. W.C., C.d.H., A.M., and P.A.S. performed experiments and collected data. W.C. conducted data analyses. M.L. implemented technical tools to assist with imaging analyses. S.L. provided expertise on beta burst analysis. P.A.S., P.S.L., and D.A.L. performed surgical procedures. W.C. wrote the original draft. All authors reviewed the manuscript.

DECLARATION OF INTERESTS

P.L. receives honoraria from Medtronic. The remaining authors declare no competing interests.

Keywords

Parkinson's disease; electrocorticography; hyperdirect pathway; prefrontal cortex; movement inhibition

INTRODUCTION

Stopping a movement that has already been initiated is critical for motor control. Movement inhibition is thought to be mediated by a "hyperdirect" monosynaptic pathway between the inferior frontal gyrus (IFG) and subthalamic nucleus (STN) (Aron et al., 2007; Nambu et al., 2002). In non-human primates, anterograde tracer studies demonstrate a lateral prefrontal projection to the ventral STN (Haynes and Haber, 2013). Due to methodological constraints, however, there is limited evidence in humans that a monosynaptic IFG-STN pathway exists or that hyperdirect activation is involved in stopping. Tractography studies have identified white matter tracts between the IFG and STN (Aron et al., 2007), although imaging lacks the ability to isolate pathways that are monosynaptic. Scalp electroencephalography (EEG) studies have identified short latency evoked potentials in the frontal-central cortex elicited from STN stimulation, indicating monosynaptic connectivity (Ashby et al., 2001; Baker et al., 2002; Walker et al., 2012). However, EEG lacks the spatial resolution to discern whether the pathway originates in the IFG or if it is a distributed pathway across the frontal-central cortex.

Functionally, the IFG and STN are thought to be involved in stopping (Aron et al., 2016), but activity in this pathway has not yet been characterized with high spatio-temporal resolution. Initial functional imaging studies indicated that blood oxygenation in the STN region and IFG were modulated during a stop signal task. *Single-site* invasive electrophysiology studies showed that beta band (~11–30 Hz) activity in the field potentials of the STN (Alegre et al., 2013; Kuhn et al., 2004; Ray et al., 2012) and IFG (Swann et al., 2009; Swann et al., 2012), assessed independently, increased during successful stopping, prompting the hypothesis that synchronized oscillatory activity in these structures mediates movement inhibition.

We utilize high-resolution, invasive electrophysiology in *both* the IFG and STN to characterize prefrontal hyperdirect topography and its functional relevance during stopping. In Parkinson's disease patients undergoing awake neurosurgery for implantation of deep brain stimulation (DBS) electrodes, we used intraoperative electrocorticography (ECoG) targeted to the IFG and DBS electrodes targeted to the STN. We performed evoked potentials experiments to characterize monosynaptic connectivity, and we used the stop signal task to characterize stopping-related activity. We provide physiological evidence for the existence of a prefrontal-subthalamic hyperdirect pathway in humans, show that IFG and STN are tightly synchronized during stopping, and that IFG-STN synchronization predicts stop signal reaction time across subjects.

RESULTS

Subjects

We enrolled 21 subjects with Parkinson's disease: 16 subjects participated in the evoked potentials experiments and 15 subjects performed the stop signal task (10 subjects participated in both) (Table S1, Table S2). Evoked potentials data from 2 subjects were excluded due to technical failures. Stop signal task data from 5 subjects were excluded due to violation of the race model, in which unsuccessful STOP reactions times were greater than successful GO reaction times (Verbruggen et al., 2019). Subjects were off dopaminergic medications for 12 hours. The mean DBS electrode coordinates for the right STN, aligned to the anterior commissure-posterior commissure line, were: 10.7 ± 0.6 (lateral), −3.5 ± 1.7 (anterior-posterior), −6.2 ± 1.4 (vertical). Coordinates for the left STN were: −11.5 ± 0.7, −3.4 ± 1.1, −7.4 ± 1.5. The mean age of subjects was 67.5 ± 6.3 years and mean disease duration was 8.6 ± 3.4 years.

STN stimulation evokes cortical potentials after ~2 ms

First, we found evidence for a prefrontal-subthalamic hyperdirect pathway in humans by stimulating in the STN and examining antidromic evoked activity in the prefrontal cortex. Short latency potentials in the cortex support the existence of a fast-conducting monosynaptic connection. Figure 1 illustrates evoked cortical activity in a single subject example. Contacts were localized both with imaging (Figure 1A,B) and electrophysiology (Figure 1C). Bipolar stimulation in the right STN in the two most ventral STN contacts evoked activity in the ipsilateral ECoG after ~2 ms (Figure 1D). Because the short latency evoked potential was small in amplitude, we summed the evoked potentials elicited from two stimulation settings with reversed anode and cathode configurations, similar to previous EEG studies (Walker et al., 2012). We quantified the amplitude of the 2 ms evoked potential to characterize the subthalamic and cortical topography of the hyperdirect pathway. We found that ventral STN stimulation elicited larger amplitude potentials than dorsal STN stimulation, suggesting stronger prefrontal-ventral STN connectivity ($p=4.0*10^{-6}$, Wilcoxon signed rank; Figure 1E). Furthermore, greater evoked potential amplitudes were found in channels covering the IFG regions compared to neighboring regions, suggesting stronger hyperdirect connectivity for the IFG than more distant cortical regions (Figure 1F).

We ruled out artifactual contributions to this short latency, low amplitude event by manipulating stimulation and recording paradigms. Reversal of the stimulating anode and cathode reversed the stimulation artifact, but not the polarity of the evoked potential (Figure 1G). We performed additional control experiments in 5 subjects. Evoked potentials scaled with stimulation current (Figure S1A), were invariant to ECoG referencing scheme (Figure S1B), were not a cumulative effect of constant 10 Hz stimulation (Figure S1C), and did not arise from pallidal stimulation (Figure S1D).

Across all subjects, we conducted matched analyses of evoked potential latency, subthalamic topography, and cortical topography. The mean latency of the earliest cortical evoked potential following STN stimulation was 2.2 ± 0.2 ms (Figure 2A). Ventral STN stimulation elicited larger amplitude evoked potentials than dorsal STN stimulation ($p=4.9*10^{-4}$,

Wilcoxon signed rank test; Figure 2B). In the cortical regions that we covered, evoked responses were greatest in the IFG and the perisylvian region of the superior temporal lobe, with a tapering of amplitudes in peripheral regions (Figure 2C, Figure S2).

Hyperdirect evoked potentials were elicited in the hemisphere ipsilateral to the stimulated STN, in subjects with left or right ECoG coverage. To compare evoked activity in both hemispheres, we evaluated evoked potentials in a single subject who received both left and right ECoG during two separate surgeries (Figure S3A). We found similar evoked responses ~2 ms after left and right STN stimulation, indicating that lateral projections to the STN are not strongly lateralized (Figure S3B). The latency of the evoked response was earlier on the right hemisphere than left ($p=5.9*10^{-4}$, Wilcoxon rank sum; Figure S3C). Cortical topography was similar on both sides (Figure S3D), with the smallest evoked responses in contacts furthest from the IFG.

Following the 2 ms potential, the next distinct cortical evoked event occurred 6.0 ± 0.35 ms after stimulation (Figure S4A). Even at this longer latency, conduction is still rapid enough to be mediated by retrograde activation of hyperdirect fibers, so we also assessed the topography of this longer latency potential. We found subjects in which the topography of the 6 ms potential clearly differed from that of the 2 ms potential, with larger amplitudes over dorsolateral prefrontal cortex than over the IFG, although in other subjects the topographies did not differ (examples in Figure S4B). Across all subjects, the 6 ms potential was more broadly distributed across the prefrontal cortex (Figure S4C). This suggests that a more “diffuse” hyperdirect pathway from widespread prefrontal areas could utilize slightly smaller diameter axons, while the largest diameter, shortest latency fibers are relatively more restricted to IFG-STN pathway (Figure 2C).

Synchronized task-related potentials in the IFG and STN are correlated with stopping speed

To characterize the role of the prefrontal-subthalamic hyperdirect pathway in movement inhibition, subjects performed a visual stop signal task (Figure 3A). In 66% of trials, a left or right arrow cued a left or right button press, respectively (GO trials). In 33% of trials, a stop cue followed the go cue after a variable delay, signaling a halt in movement (STOP trials). Across all subjects, mean GO trial accuracy was 86 ± 10% and mean STOP accuracy was 66 ± 11% (Figure 3B). Mean GO reaction time was 779 ± 193 ms, mean stop signal delay was 441 ± 209 ms, and estimated stop signal reaction time was 384 ± 76 ms (Figure 3B).

We generated event-related potentials (ERPs) of cortical and STN evoked activity during the task. After the STOP cue in successful stop trials, ERP deflections appear in both the cortex and STN after ~200–300 ms (Figure 3C). To quantify the lag between cortical and subthalamic ERPs, we calculated the cross correlation (Figure 3D). Across subjects, the average cross correlation lag between all cortical-STN channel pairs was −90 ± 131 ms, with cortex leading the STN ($p=0.029$, t-test; Figure 3E). We validated our metric for prefrontal-STN lag by quantifying the temporal offset of cortical and STN ERPs with one alternative method. In ECoG and STN channels where we could identify distinct, matching ERP deflections, we calculated the difference in time between the deflection onset (maximum

point in the upward deflection). Both calculations of cortico-STN ERP latency offset indicate that cortical activity precedes subthalamic activity during stopping (Figure 3E).

Next, we asked if the degree of circuit co-activation was linked to behavior. The mean prefrontal-subthalamic correlation across subjects was 0.46 ± 0.15 (Figure 3F). Across subjects, the degree of correlation was inversely related to the stop signal reaction time ($p=0.040$, $r=0.65$, Spearman correlation; Figure 3G), suggesting that greater hyperdirect circuit activity is linked to faster stopping. Although movement inhibition is impaired in Parkinson's disease (Gauggel et al., 2004), we did not find physiology or stopping behaviors to be correlated with Parkinsonian severity: subjects' total scores on the Unified Parkinson's Disease Rating Scale were not correlated with the stop signal reaction time ($p=0.82$, $r=0.084$, Pearson correlation) or with cortico-STN correlation during stopping ($p=0.72$, $r=0.13$, Pearson correlation).

Within subjects, we looked for physiological predictors of behavior that would differentiate between successful and failed stop trials. We hypothesized three different models that could produce success vs. failure: 1) IFG-STN activity is more correlated during successful stopping, 2) IFG-STN lag is shorter during successful stopping, or 3) IFG-STN activity is initiated more quickly during successful stopping. Within subjects, we did not find differences in cortico-subthalamic correlation ($p=0.73$, t-test; Figure S5A) or IFG-STN lag ($p=0.93$, t-test; Figure S5B) during successful vs. failed stopping. We found that cortical ERPs during successful stopping preceded activity during failed stopping within subjects, with a mean lag of −12 ± 21 ms ($p=0.050$, one sample t-test; Figure S5C), suggesting that faster initiation of IFG-STN activity is important for successful stopping.

IFG and STN modulate delta and beta frequencies during successful stopping

Previous studies characterizing single-site activity in either the IFG or the STN during stopping have linked modulations of beta power to successful stopping (Alegre et al., 2013; Kuhn et al., 2004; Ray et al., 2012; Swann et al., 2009; Swann et al., 2012). We therefore conducted frequency domain analyses to characterize stopping related oscillatory activity in the IFG and STN and stopping related coherence between these structures.

Figure 4A illustrates activity in a single cortical and single STN channel for an example patient. In single trials, delta activity in the IFG and STN increases immediately after the stop cue. The onset of delta power modulation has a consistent temporal relationship with the onset of the STOP cue, and it does not appear after the GO cue (Figure S6A), suggesting that it is a modulation specific to the stopping process. Beta power decreases after the GO cue, and then increases after the STOP cue in the IFG and STN (Figure 4A, Figure S6A). These delta and beta modulations were significant in the trial-averaged spectrograms (Figure S6). The increase in beta power occurred after the estimated time of stopping. Pooled activity across all subjects show similar modulations in the grand-averaged spectrograms (Figure 4B). We used the grand average spectrograms to characterize the cortical topography of stopping-related activity. In the regions covered, the IFG had the greatest task-related delta and beta power ($p<0.05$ multifactorial ANOVA, with post-hoc Tukey's HSD pairwise comparisons; Figure 4C).

Since stopping-related delta activity in the frequency domain analyses is of short duration, it does not necessarily reflect an oscillatory phenomenon. This frequency domain modulation likely reflects the same ERP captured in the time domain. In support of this, task-evoked delta power was correlated with amplitude of the ERP ($p=0.03$, $r=0.17$, Spearman correlation; Figure 4D).

Finally, we asked whether beta modulations in IFG and STN, or coherent beta band interactions between IFG and STN, predicted stopping behaviors, either between or within subjects. Beta power at each site individually, quantified in the 13–30 Hz range and in 250 ms window before and after the SSRT, was not predictive of SSRT (Bonferroni-corrected $p>0.05$, Spearman correlation). Next, we analyzed beta in subject-specific narrow frequency bands, assessing beta amplitude and beta bursts in both the IFG and STN. Beta amplitude, burst rate, burst size, and burst duration (Hannah et al., 2019) in both sites were not predictive of SSRT independently (Bonferroni-corrected $p>0.05$, Spearman correlation), or in a combined multivariate regression model ($p=0.22$, $R^2=0.35$). Within subjects, these metrics also did not differentiate successful vs. failed stopping (Bonferroni-corrected $p>0.05$, Wilcoxon signed rank). Furthermore, we did not find that beta amplitude or beta bursts were predictive of GO reaction times in either the IFG or STN (Bonferroni-corrected $p>0.05$, Spearman correlation).

Oscillatory coherence between the IFG and STN was also not predictive of SSRT in the beta band ($p=0.57$, $r=-0.21$, Spearman correlation; Figure 4E), or in any other frequency range (Figure S7). We also looked for oscillatory interactions between IFG and STN by analyzing the power spectrum of the time-domain measure of synchronization discussed above, the cross correlation of the IFG and STN ERPs. These power spectra were calculated across all contact pairs then averaged for each patient. We found some patients with a visible peak in the beta band, consistent with an oscillatory coherence between prefrontal cortex and STN during stopping, though not all patients showed this peak (examples in Figure S8). However, there was no difference in SSRT between patients with and without a beta peak ($p=0.062$, Wilcoxon rank sum). Thus, in this population of PD patients off of dopaminergic medication, we did not find evidence for a relationship between beta modulation and stopping or going in this circuit.

DISCUSSION

We used invasive brain recordings in Parkinson’s disease patients to characterize the IFG-STN circuit and its activity during stopping. By stimulating in the STN and recording in prefrontal cortex, we identified a fast evoked potential that provides the first physiological evidence of hyperdirect (monosynaptic) connectivity between the IFG and ventral STN in humans. During a stop signal task, we show correlated stopping-related evoked activity in both the IFG and STN, and the degree of co-activation of these structures is predictive of stopping speed across subjects. Although we did find increases in IFG and STN beta at the estimated time of stopping, beta coherence was not correlated with stopping speed. Our study is the first to show that the hyperdirect circuit co-modulation is linked to stopping behaviors, which has broad implications for stimulation-based therapies to treat maladaptive movement inhibition.

Short latency evoked potentials identify a prefrontal-subthalamic hyperdirect pathway in humans

The hyperdirect pathway was initially proposed to be a rapid connection from motor cortical regions to the STN, bypassing the striatum and providing rapid modulation of basal ganglia output (Nambu et al., 2002). Subthalamic innervation from primary motor, supplementary motor, and premotor afferents was first identified in non-human primates using electrophysiological and histological techniques (Monakow et al., 1978; Nambu et al., 1996; Nambu et al., 1997). In humans, subthalamic stimulation elicits fast latency evoked potentials in *motor* cortical regions, recorded using EEG (Ashby et al., 2001; Baker et al., 2002; Walker et al., 2012) and ECoG (Kelley et al., 2018; Miocinovic et al., 2018), consistent with retrograde activation of a hyperdirect pathway. More recently, attention has focused on a possible *prefrontal*-subthalamic pathway and its role in the cognitive control of inhibition. Histological tracing in non-human primates have identified prefrontal projections to the STN, with a topography favoring more ventral regions of the STN (Haynes and Haber, 2013). However, there has been limited anatomic or physiological characterization of this pathway in humans.

Our study is the first to use invasive electrodes at both the origin and the termination of the prefrontal-subthalamic hyperdirect pathway to show monosynaptic connectivity. Consistent with evoked potentials latencies reported in the EEG literature, we found an average latency of 2.2 ms for the earliest evoked event across all subjects. This evoked potential likely reflects rapid axonal back-propagation, with a conduction time of about 25 m/s, assuming a 5 cm distance between the prefrontal cortex and STN. These fibers are slower than the large axon fibers of corticospinal tract, which have conduction velocities of 41 m/s (Ashby et al., 1998). This is consistent with rodent tract tracing studies showing that corticospinal fibers that collateralize to the STN have smaller diameter fibers than corticospinal axons that do not collateralize (Kita and Kita, 2012). We also found a longer latency evoked potential at 6 ms, suggesting hyperdirect fibers of different conduction velocities. Although a monosynaptic projection of opposite directionality (STN to cortex) has been identified histologically in rats (Degos et al., 2008; Jackson and Crossman, 1981; Kita and Kitai, 1987), evoked potentials at 2 ms and 6 ms are too fast to include both axonal conduction and trans-synaptic events.

Using evoked potential amplitude as a surrogate metric for the density of axons extending from the cortex to the STN (Buzsaki et al., 2012), we found that IFG regions had preferential innervation with the faster hyperdirect fibers (2 ms latency) compared to neighboring regions, including the rostral middle frontal area and portions of the superior temporal lobe (Figure 2C). Evoked potentials from contacts covering superior temporal lobe likely arise from IFG activation within the Sylvian fissure rather than from the temporal lobe itself. The 6 ms evoked potential had a broader topographic distribution across the prefrontal cortex, consistent with nonhuman primate tracing studies suggesting broad prefrontal cortical innervation (Haynes and Haber, 2013). Furthermore, we found a topography of stronger prefrontal projections to the ventral STN, consistent with anatomical (Haynes and Haber, 2013) and functional (Pasquereau and Turner, 2017) evidence from nonhuman primates. Dorsal STN stimulation did evoke the hyperdirect potential, but at a smaller

amplitude. This may arise from current spread in this small nucleus, or from incomplete segregation of motor and nonmotor pathways (Haynes and Haber, 2013).

IFG-STN hyperdirect pathway mediates rapid movement inhibition

The IFG and STN are thought to be involved in stopping, but we have lacked precise physiological characterization of circuit activity during stopping in humans. Initial functional imaging studies found increased blood oxygenation in IFG, STN, and pre-SMA during successful stopping (Aron et al., 2007; Aron and Poldrack, 2006; Chambers et al., 2009). Subsequent invasive studies in humans benefitted from higher temporal resolution recordings, but only had coverage of either the IFG or STN. In each site, assessed independently, successful stopping was associated with increased beta activity (Alegre et al., 2013; Kuhn et al., 2004; Ray et al., 2012; Swann et al., 2009; Swann et al., 2012), leading to the hypothesis that coherent beta activity between the IFG and STN mediates hyperdirect stopping.

We provide the first human evidence of IFG-STN communication consistent with hyperdirect modulation of stopping. First, the topography of stopping-related cortical activation coincided with that of hyperdirect connectivity, with both centered in the IFG (Figure 2C, Figure 4C). Second, a task-evoked potential (probably corresponding to delta modulation in the frequency domain) appeared after the stop cue but before the estimated time of stopping. Cortical and subthalamic ERPs were highly correlated, with cortical activity leading the STN. Third, synchronization of evoked activity in the IFG and STN predicted faster stopping (Figure 3G), indicating a link between stopping behavior and activation of the hyperdirect pathway.

Similar to prior single site electrophysiology studies (Alegre et al., 2013; Kuhn et al., 2004; Ray et al., 2012; Swann et al., 2009; Swann et al., 2012), we also found increases in cortical and subthalamic beta band power during successful stopping. The beta modulation was strongest in IFG regions (Figure 4C). However, we did not find a relationship between IFG-STN coherence and stopping speed or successful versus failed stopping. In addition, stopping related beta increases in IFG tended to occur later than the estimated time of stopping, whereas an electrocorticography study in patients undergoing invasive monitoring for epilepsy showed an earlier onset of the stopping-related beta increase (Swann et al., 2009). While our data support a model in which IFG-STN interaction is mediated *primarily* by a fast evoked potential rather than by oscillatory synchronization, the Parkinsonian state does perturb beta band activity in the classical thalamocortical motor loop (Brittain and Brown, 2014), and might likewise do so in the prefrontal cortex. This could reduce or delay a putative beta-band modulation of hyperdirect stopping. Although levodopa medication is not thought to affect SSRT (Obeso et al., 2011), our subjects' GO and STOP reaction times are slower than those previously reported, and Parkinson's disease is associated with deficits in behavioral inhibition (Frank et al., 2007; Jahanshahi et al., 2015). Alternatively, if not causally involved in stopping, the beta modulation in the IFG and STN may reflect a rebound of activity related to action termination, which has been described in other regions involved in motor control, such as the sensorimotor cortex (Crone et al., 1998; Kuhn et al.,

2004), supplementary motor area (Ohara, 2000), STN (Kuhn et al., 2004), and putamen (Sochurkova and Rektor, 2003).

The prefrontal hyperdirect pathway is likely to function as a brake during inhibitory processes beyond those probed in the stop signal task, such as during decision conflict (Frank et al., 2007; Zavala et al., 2016; Zavala et al., 2014) and during surprising events (Wessel and Aron, 2013). Thus a better understanding of the hyperdirect pathway is important for developing therapies to treat maladaptive behavioral inhibition, such as freezing of gait in Parkinson's disease. Direct cortico-STN projections are thought to be perturbed in Parkinson's (Chu et al., 2017), and one therapeutic mechanisms of STN DBS is hypothesized to arise from altering hyperdirect activity (Gradinaru et al., 2009). Modulation of stopping-related activity in this pathway may be therapeutic.

STAR METHODS

Lead Contact and Materials Availability

Further information and requests for resources should be directed to and will be fulfilled by the Lead Contact, Philip Starr (philip.starr@ucsf.edu). This study did not generate new unique reagents.

Experimental Model and Subjects Details

We enrolled 21 subjects with Parkinson's disease (19 male/2 female) with a clinical indication for DBS surgery (Table S1, Table S2). Subjects were recruited from the University of California San Francisco and the San Francisco Veterans Affairs Health Care System. Inclusion criteria were: diagnosis of idiopathic Parkinson's disease confirmed by movement disorders neurologists, primary rigid-akinetic motor phenotype, Unified Parkinson's Disease Rating Scale Part III score ≥ 30, and motor fluctuations on vs. off dopaminergic medications. The mean age of subjects was 67.5 ± 6.3 years and mean disease duration was 8.6 ± 3.4 years. Patients were off Parkinsonian medications for at least 12 hours prior to surgery. All patients consented to have a temporary ECoG strip for research purposes during their DBS surgeries. Subjects provided informed consent prior to surgery, per protocol approved by the Institutional Review Board.

Method Details

DBS and ECoG placement—Unilateral neural recordings were collected from each subject, with a DBS electrode targeted to the basal ganglia and ECoG electrodes targeted to the inferior frontal cortex. The ECoG strip was placed ipsilateral to the DBS electrode.

Subjects had DBS electrodes targeted to the STN, GPi, or the ventralis intermedius nucleus of the thalamus. While the STN was the primary subcortical region studied, some subjects with pallidal and thalamic electrodes were also studied for comparison. STN DBS leads contain 4 electrodes of 1.5 mm length and 1.27 mm diameter, spaced 0.5 mm apart (Medtronic Model 3389), and GPi and thalamic leads contain 4 electrodes of 1.5 mm length and 1.27 mm diameter, spaced 1.5 mm apart (Medtronic Model 3387). DBS electrodes were placed under standard surgical protocol (Starr, 2002). The intended depth of STN leads was

determined by the location of the dorsal and ventral borders of STN, mapped intraoperatively by single unit microelectrode recordings (Starr, 2002). The most dorsal contact (contact 3) was placed outside of, and immediately dorsal to, the dorsal border of the STN. Contact 2 was placed in the dorsal (motor) territory of the STN; while contacts 1 and 0 were in the ventral STN.

A temporary, high-resolution, subdural ECoG strip (Ad-tech, Racine, WI) was inserted in the cortex ipsilateral to the STN electrode, through the same 15 mm burr hole used for DBS insertion (Panov et al., 2017). The 28-contact ECoG strip consisted of 2 rows of 14 contacts. Each contact was 1.2 mm in diameter and spaced 4 mm center-to-center. The strip was targeted to one of the three regions of the IFG: pars opercularis, pars triangularis, or pars orbitalis. Stereotactic targeting was performed with preoperative MRI using surgical planning software (Medtronic Framelink v5.1, Minneapolis, MN). Neural recordings began at least 30 min after cessation of propofol, after which it does not affect neuronal activity (Herrick et al., 1997; Raz et al., 2010). No other sedatives were used during awake neural recordings.

Anatomic localization of electrodes—To anatomically localize ECoG and basal ganglia contacts, we fused intraoperative CT images with the preoperative MRI (Panov et al., 2017). The preoperative T1 MRI was used to reconstruct individual cortical surface models in FreeSurfer (Dale et al., 1999; Fischl et al., 2002). We projected ECoG contacts on to the cortical surface mesh using the *img_pipe* toolbox (Hamilton et al., 2017) and a surface vector projection method (Kubanek and Schalk, 2015). Individual cortical surfaces were fit to the Desikan-Killiany atlas brain to generate cortical anatomy labels for each ECoG contact (Desikan et al., 2006).

Evoked potentials stimulation—To assess hyperdirect topography in the STN, each subject received ventral and dorsal STN stimulation while ipsilateral cortical activity was recorded. Each stimulation block was 30 s in duration, using 10 Hz pulses and biphasic square waves with 100 μs pulse width. We tested multiple stimulation settings at each site, varying the stimulation current and electrode configuration, to ensure that evoked potentials were not artifactual. We tested stepped stimulation currents between 3 and 6 mA to see if evoked responses scaled with current. We tested stimulation paradigms that reversed the polarity of the stimulation artifact and assessed the polarity of the evoked potentials. For bipolar stimulation, we reversed the cathode/anode configuration. For monopolar stimulation, we tested two biphasic square wave designs: negative phase followed by positive phase and vice versa.

Stop signal task—A visual stop signal task was programmed using PsychToolbox for MATLAB (Mathworks, Natick, MA). Subjects performed 196–288 total trials, depending on intraoperative time constraints. During GO trials (66% of all trials), subjects were presented with an arrow pointing left or right, instructing a left or right button press, respectively. Subjects performed the task with the hand ipsilateral to the recorded side, unless there was significant tremor in that hand. During STOP trials (33% of all trials), a stop cue appeared after a variable stop signal delay, and subjects were instructed to halt movement. A staircase

procedure was used to adjust stop signal delays in order to achieve approximately 50% stopping success for each subject (Verbruggen et al., 2019).

Signal recordings—Evoked potential experiments were conducted using the Neuro Omega system (Alpha Omega, Nazareth, Israel), which delivered stimulation through the STN channels and simultaneously recorded ECoG potentials. Custom MATLAB scripts were written to implement stimulation. The Neuro Omega signals were recorded at a 22 KHz sampling rate and 0.075– 3500 Hz bandpass filtered. Neural data during the stop signal task were collected on either the Neuro Omega or TDT PZ5 (Tucker Davis Technologies, Alachua, FL). The TDT signals were recorded at 3 kHz and 0.45–1350 Hz bandpass filtered. We recorded ECoG potentials with two different referencing schemes to rule out the contributions of the reference electrodes to the evoked potentials. All ECoG potentials were recorded referenced to either an ipsilateral scalp needle placed subcutaneously in the vertex or scalp needles placed bilaterally in the mastoids.

Evoked potentials analysis—To generate the cortical responses to subthalamic stimulation, 250 of the 300 total ECoG epochs were time-locked to stimulation and averaged. The 50 trials near the onset and offset of the entire stimulation block were discarded due to potential artifacts. The evoked responses were smoothed using a moving average filter. Peaks and troughs, and their associated amplitudes, were identified using MATLAB function *findpeaks*. To normalize evoked potential amplitudes per patient, the largest amplitude evoked potential was identified per ECoG strip. All other evoked potential amplitudes across the ECoG strip were normalized as a percentage of that maximum evoked potential. We excluded ECoG electrodes with high impedances or high amplitude noise.

Stop signal task analysis—Behavioral data were analyzed to ensure that the assumptions of the race model were met. Subjects were excluded when their mean unsuccessful STOP reactions times were greater than their mean successful GO reaction times (Verbruggen et al., 2019). In subjects who did not violate the race model, the stop signal reaction time was estimated by subtracting the mean stop signal delay from the mean go reaction time.

Temporal and spectral properties of the neural data were assessed during the task. To generate event-related potentials (ERPs), time series data were first low pass filtered below 250 Hz to remove high frequency intraoperative noise. Epochs of ECoG and STN potentials were time-locked to the STOP cue and averaged. To assess the similarity and time lag of cortical and STN potentials, cross correlations were generated for the averaged ECoG and STN ERPs. Statistical analyses of cross correlations were performed using bootstrapping, with 10000 surrogate cross-correlations time-locked to shuffled points. To verify the lag calculated using cross correlations, the temporal offset between cortical and STN ERPs were also calculated with a second method: in channel pairs where we could identify distinct matching deflections in the ERPs, we calculated the time lag between the maxima of the deflections in the cortex and the STN. Spectral properties of the cross-correlations were assessed by calculating the power spectral density using Welch’s periodogram.

To generate task-related spectrograms, data were down-sampled to 1000 Hz. Frequency decomposition was performed using wavelet convolution (Canolty et al., 2007). Data were filtered with Gabor wavelets into 128 center frequencies ranging from 2.5–250 Hz. Epochs of data were time-locked to either the GO or STOP cue. We randomly sub-selected the trials for each condition to equalize the total number of trials that contributed to GO and STOP spectrograms. The epochs were averaged and each frequency in the spectrogram was baseline corrected by subtracting the average power of a 500 ms window in the preceding inter-trial interval. Spectrograms were z-score normalized with bootstrapping: we generated a surrogate distribution of task-related activity time-locked to 10000 shuffled points. Within subjects, an average spectrogram per anatomic region was calculated by averaging all contacts within the same region. Grand averaged spectrograms were then generated by averaging across all patients. Task-related power was quantified for the following frequency ranges: delta (1–4 Hz), theta (4–8 Hz), alpha (8–13 Hz), beta (13–30 Hz), gamma (50–150 Hz). To calculate task-related coherence, we calculated beta coherence between each IFG contact and the ventral STN in each subject. We averaged coherence in all channel pairs per patient.

For analysis of patient-specific narrow band beta modulation, we first identified the channel with the maximum task-modulated beta power per patient: based on the z-scored trial-averaged spectrograms, we selected the channel with the maximum mean 13–30 Hz beta modulation in the 500 window surrounding the SSRT. For this single channel per patient, we specified a patient-specific narrow band beta by identifying the maximum frequency in the peak of the power spectra, within the 13–30 Hz range. We took a 6 Hz window around that peak frequency and filtered the data in that frequency band. Beta burst thresholds were identified using the empirical method (Shin et al., 2017) and bursts were identified as events that crossed that threshold. We quantified beta amplitude, burst rate, burst size, and burst duration across all trials in the 250 ms window before and after the SSRT and as well as before and after the GO RT. These metrics were averaged across trials per patient.

Quantification and Statistical Analysis

Data are represented as mean ± standard deviation. Kolmogorov-Smirnov tests for normality were used to determine whether parametric (t-test) or non-parametric (Wilcoxon signed rank, Wilcoxon rank sum) statistical tests were used. Pearson correlation was used for correlations between two continuous variables, and Spearman correlation was used for correlations involving ordinal variables. Bootstrapping was used to identify significant task-related modulations. A p-value < 0.05 (corrected for multiple comparisons where appropriate) was considered statistically significant. Statistical tests are reported in the main text.

Data and Code Availability

The datasets supporting the current study have not been deposited in a public repository because they contain patient information, but are available from the Lead Author on request.

Supplementary Material

Refer to Web version on PubMed Central for supplementary material.

ACKNOWLEDGEMENTS

This work was supported by the National Institutes of Health (F31 NS103410-01A1).

REFERENCES

Alegre M, Lopez-Azcarate J, Obeso I, Wilkinson L, Rodriguez-Oroz MC, Valencia M, Garcia-Garcia D, Guridi J, Artieda J, Jahanshahi M, and Obeso JA (2013). The subthalamic nucleus is involved in successful inhibition in the stop-signal task: a local field potential study in Parkinson's disease. Exp Neurol 239, 1–12. [PubMed: 22975442]

Aron AR, Behrens TE, Smith S, Frank MJ, and Poldrack RA (2007). Triangulating a cognitive control network using diffusion-weighted magnetic resonance imaging (MRI) and functional MRI. J Neurosci 27, 3743–3752. [PubMed: 17409238]

Aron AR, Herz DM, Brown P, Forstmann BU, and Zaghloul K (2016). Frontosubthalamic Circuits for Control of Action and Cognition. J Neurosci 36, 11489–11495. [PubMed: 27911752]

Aron AR, and Poldrack RA (2006). Cortical and subcortical contributions to Stop signal response inhibition: role of the subthalamic nucleus. J Neurosci 26, 2424–2433. [PubMed: 16510720]

Ashby P, Paradiso G, Saint-Cyr JA, Chen R, Lang AE, and Lozano AM (2001). Potentials recorded at the scalp by stimulation near the human subthalamic nucleus. Clinical Neurophysiology 112, 431–437. [PubMed: 11222963]

Ashby P, Strafella A, Dostrovsky JO, Lozano A, and Lang AE (1998). Immediate motor effects of stimulation through electrodes implanted in the human globus pallidus. Stereotact Funct Neurosurg 70, 1–18. [PubMed: 9691237]

Baker KB, Montgomery EB Jr., Rezai AR, Burgess R, and Luders HO (2002). Subthalamic nucleus deep brain stimulus evoked potentials: physiological and therapeutic implications. Mov Disord 17, 969–983. [PubMed: 12360546]

Brittain JS, and Brown P (2014). Oscillations and the basal ganglia: motor control and beyond. Neuroimage 85 Pt 2, 637–647.

Buzsaki G, Anastassiou CA, and Koch C (2012). The origin of extracellular fields and currents--EEG, ECoG, LFP and spikes. Nat Rev Neurosci 13, 407–420. [PubMed: 22595786]

Canolty RT, Soltani M, Dalal SS, Edwards E, Dronkers NF, Nagarajan SS, Kirsch HE, Barbaro NM, and Knight RT (2007). Spatiotemporal dynamics of word processing in the human brain. Front Neurosci 1, 185–196. [PubMed: 18982128]

Chambers CD, Garavan H, and Bellgrove MA (2009). Insights into the neural basis of response inhibition from cognitive and clinical neuroscience. Neurosci Biobehav Rev 33, 631–646. [PubMed: 18835296]

Chu HY, McIver EL, Kovaleski RF, Atherton JF, and Bevan MD (2017). Loss of Hyperdirect Pathway Cortico-Subthalamic Inputs Following Degeneration of Midbrain Dopamine Neurons. Neuron 95, 1306–1318 e1305. [PubMed: 28910619]

Crone NE, Miglioretti DL, Gordon B, Sieracki JM, Wilson MT, Uematsu S, and Lesser RP (1998). Functional mapping of human sensorimotor cortex with electrocorticographic spectral analysis. I. Alpha and beta event-related desynchronization. Brain 121 (Pt 12), 2271–2299. [PubMed: 9874480]

Dale AM, Fischl B, and Sereno MI (1999). Cortical surface-based analysis. I. Segmentation and surface reconstruction. Neuroimage 9, 179–194. [PubMed: 9931268]

Degos B, Deniau JM, Le Cam J, Mailly P, and Maurice N (2008). Evidence for a direct subthalamo-cortical loop circuit in the rat. Eur J Neurosci 27, 2599–2610. [PubMed: 18547246]

Desikan RS, Segonne F, Fischl B, Quinn BT, Dickerson BC, Blacker D, Buckner RL, Dale AM, Maguire RP, Hyman BT, et al. (2006). An automated labeling system for subdividing the human

cerebral cortex on MRI scans into gyral based regions of interest. Neuroimage 31, 968–980. [PubMed: 16530430]

Fischl B, Salat DH, Busa E, Albert M, Dieterich M, Haselgrove C, van der Kouwe A, Killiany R, Kennedy D, Klaveness S, et al. (2002). Whole brain segmentation: automated labeling of neuroanatomical structures in the human brain. Neuron 33, 341–355. [PubMed: 11832223]

Frank MJ, Samanta J, Moustafa AA, and Sherman SJ (2007). Hold your horses: impulsivity, deep brain stimulation, and medication in parkinsonism. Science 318, 1309–1312. [PubMed: 17962524]

Gauggel S, Rieger M, and Feghoff TA (2004). Inhibition of ongoing responses in patients with Parkinson's disease. J Neurol Neurosurg Psychiatry 75, 539–544. [PubMed: 15026491]

Gradinaru V, Mogri M, Thompson KR, Henderson JM, and Deisseroth K (2009). Optical deconstruction of parkinsonian neural circuitry. Science 324, 354–359. [PubMed: 19299587]

Hamilton LS, Chang DL, Lee MB, and Chang EF (2017). Semi-automated Anatomical Labeling and Inter-subject Warping of High-Density Intracranial Recording Electrodes in Electrocorticography. Front Neuroinform 11, 62. [PubMed: 29163118]

Hannah R, Muralidharan V, Sundby KK, and Aron AR (2019). Temporally-precise disruption of prefrontal cortex informed by the timing of beta bursts impairs human action-stopping. bioRxiv.

Haynes WI, and Haber SN (2013). The organization of prefrontal-subthalamic inputs in primates provides an anatomical substrate for both functional specificity and integration: implications for Basal Ganglia models and deep brain stimulation. J Neurosci 33, 4804–4814. [PubMed: 23486951]

Herrick IA, Craen RA, Gelb AW, McLachlan RS, Girvin JP, Parrent AG, Eliasziw M, and Kirkby J (1997). Propofol sedation during awake craniotomy for seizures: electrocorticographic and epileptogenic effects. Anesth Analg 84, 1280–1284. [PubMed: 9174307]

Jackson A, and Crossman AR (1981). Subthalamic nucleus efferent projection to the cerebral cortex. Neuroscience 6, 2367–2377. [PubMed: 7329552]

Jahanshahi M, Obeso I, Baunez C, Alegre M, and Krack P (2015). Parkinson's disease, the subthalamic nucleus, inhibition, and impulsivity. Mov Disord 30, 128–140. [PubMed: 25297382]

Kelley R, Flouty O, Emmons EB, Kim Y, Kingyon J, Wessel JR, Oya H, Greenlee JD, and Narayanan NS (2018). A human prefrontal-subthalamic circuit for cognitive control. Brain 141, 205–216. [PubMed: 29190362]

Kita H, and Kitai ST (1987). Efferent projections of the subthalamic nucleus in the rat: light and electron microscopic analysis with the PHA-L method. J Comp Neurol 260, 435–452. [PubMed: 2439552]

Kita T, and Kita H (2012). The subthalamic nucleus is one of multiple innervation sites for long-range corticofugal axons: a single-axon tracing study in the rat. J Neurosci 32, 5990–5999. [PubMed: 22539859]

Kubanek J, and Schalk G (2015). NeuralAct: A Tool to Visualize Electrocortical (ECoG) Activity on a Three-Dimensional Model of the Cortex. Neuroinformatics 13, 167–174. [PubMed: 25381641]

Kuhn AA, Williams D, Kupsch A, Limousin P, Hariz M, Schneider GH, Yarrow K, and Brown P (2004). Event-related beta desynchronization in human subthalamic nucleus correlates with motor performance. Brain 127, 735–746. [PubMed: 14960502]

Miocinovic S, de Hemptinne C, Chen W, Isbaine F, Willie JT, Ostrem JL, and Starr PA (2018). Cortical Potentials Evoked by Subthalamic Stimulation Demonstrate a Short Latency Hyperdirect Pathway in Humans. J Neurosci 38, 9129–9141. [PubMed: 30201770]

Monakow KH, Akert K, and Kunzle H (1978). Projections of the precentral motor cortex and other cortical areas of the frontal lobe to the subthalamic nucleus in the monkey. Exp Brain Res 33, 395–403. [PubMed: 83239]

Nambu A, Takada M, Inase M, and Tokuno H (1996). Dual somatotopical representations in the primate subthalamic nucleus: evidence for ordered but reversed body-map transformations from the primary motor cortex and the supplementary motor area. The Journal of Neuroscience 16, 2671–2683. [PubMed: 8786443]

Nambu A, Tokuno H, Inase M, and Takada M (1997). Cortico-subthalamic input zones from forelimb representations of the dorsal and ventral divisions of the premotor cortex in the macaque monkey:

comparison with the input zones from the primary motor cortex and the supplementary motor area. Neuroscience Letters 239, 13–16. [PubMed: 9547160]

Nambu A, Tokuno H, and Takada M (2002). Functional significance of the cortico– subthalamo–pallidal 'hyperdirect' pathway. Neuroscience Research 43, 111–117. [PubMed: 12067746]

Obeso I, Wilkinson L, and Jahanshahi M (2011). Levodopa medication does not influence motor inhibition or conflict resolution in a conditional stop-signal task in Parkinson's disease. Exp Brain Res 213, 435–445. [PubMed: 21796541]

Ohara S (2000). Movement-related change of electrocorticographic activity in human supplementary motor area proper. Brain 123, 1203–1215. [PubMed: 10825358]

Panov F, Levin E, de Hemptinne C, Swann NC, Qasim S, Miocinovic S, Ostrem JL, and Starr PA (2017). Intraoperative electrocorticography for physiological research in movement disorders: principles and experience in 200 cases. J Neurosurg 126, 122–131. [PubMed: 26918474]

Pasquereau B, and Turner RS (2017). A selective role for ventromedial subthalamic nucleus in inhibitory control. Elife 6.

Ray NJ, Brittain JS, Holland P, Joundi RA, Stein JF, Aziz TZ, and Jenkinson N (2012). The role of the subthalamic nucleus in response inhibition: evidence from local field potential recordings in the human subthalamic nucleus. Neuroimage 60, 271–278. [PubMed: 22209815]

Raz A, Eimerl D, Zaidel A, Bergman H, and Israel Z (2010). Propofol decreases neuronal population spiking activity in the subthalamic nucleus of Parkinsonian patients. Anesth Analg 111, 1285–1289. [PubMed: 20841416]

Shin H, Law R, Tsutsui S, Moore CI, and Jones SR (2017). The rate of transient beta frequency events predicts behavior across tasks and species. Elife 6.

Sochurkova D, and Rektor I (2003). Event-related desynchronization/synchronization in the putamen. An SEEG case study. Exp Brain Res 149, 401–404. [PubMed: 12632243]

Starr PA (2002). Placement of deep brain stimulators into the subthalamic nucleus or Globus pallidus internus: technical approach. Stereotact Funct Neurosurg 79, 118–145. [PubMed: 12890973]

Swann N, Tandon N, Canolty R, Ellmore TM, McEvoy LK, Dreyer S, DiSano M, and Aron AR (2009). Intracranial EEG reveals a time- and frequency-specific role for the right inferior frontal gyrus and primary motor cortex in stopping initiated responses. J Neurosci 29, 12675–12685. [PubMed: 19812342]

Swann NC, Cai W, Conner CR, Pieters TA, Claffey MP, George JS, Aron AR, and Tandon N (2012). Roles for the pre-supplementary motor area and the right inferior frontal gyrus in stopping action: electrophysiological responses and functional and structural connectivity. Neuroimage 59, 2860–2870. [PubMed: 21979383]

Verbruggen F, Aron AR, Band GP, Beste C, Bissett PG, Brockett AT, Brown JW, Chamberlain SR, Chambers CD, Colonius H, et al. (2019). A consensus guide to capturing the ability to inhibit actions and impulsive behaviors in the stop-signal task. Elife 8.

Walker HC, Huang H, Gonzalez CL, Bryant JE, Killen J, Cutter GR, Knowlton RC, Montgomery EB, Guthrie BL, and Watts RL (2012). Short latency activation of cortex during clinically effective subthalamic deep brain stimulation for Parkinson's disease. Mov Disord 27, 864–873. [PubMed: 22648508]

Wessel JR, and Aron AR (2013). Unexpected events induce motor slowing via a brain mechanism for action-stopping with global suppressive effects. J Neurosci 33, 18481–18491. [PubMed: 24259571]

Zavala B, Tan H, Ashkan K, Foltynie T, Limousin P, Zrinzo L, Zaghloul K, and Brown P (2016). Human subthalamic nucleus-medial frontal cortex theta phase coherence is involved in conflict and error related cortical monitoring. Neuroimage 137, 178–187. [PubMed: 27181763]

Zavala BA, Tan H, Little S, Ashkan K, Hariz M, Foltynie T, Zrinzo L, Zaghloul KA, and Brown P (2014). Midline frontal cortex low-frequency activity drives subthalamic nucleus oscillations during conflict. J Neurosci 34, 7322–7333. [PubMed: 24849364]

Author Manuscript

Author Manuscript

Author Manuscript

HIGHLIGHTS

- Demonstration of a monosynaptic, prefrontal hyperdirect pathway in humans
- Fastest fibers between the inferior frontal gyrus and ventral subthalamic nucleus
- Stopping elicits co-activation of the origin and target of this pathway
- Degree of co-activation predicts stopping speed

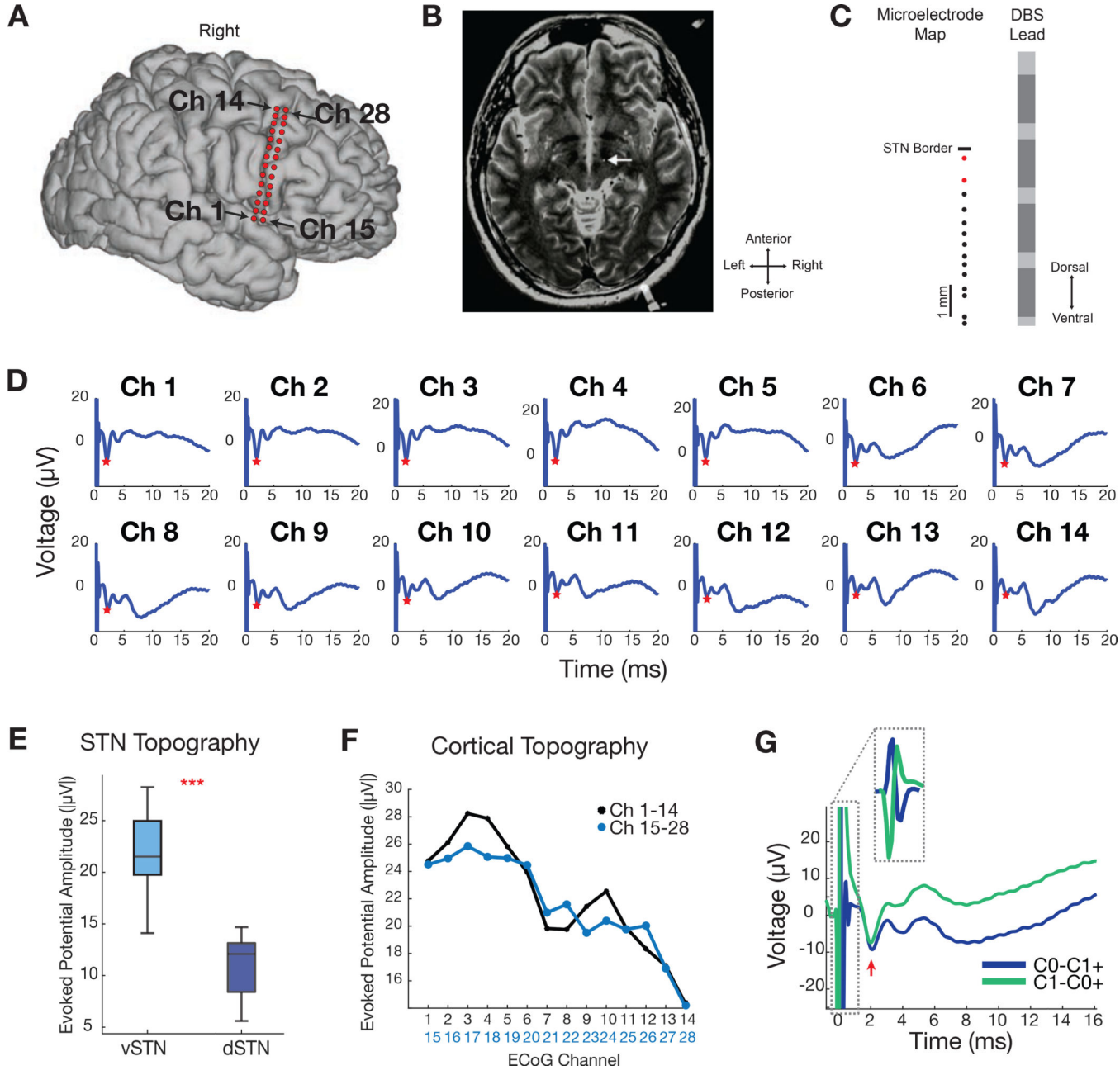

Figure 1.

A fast cortical potential evoked by STN stimulation demonstrates retrograde hyperdirect activation (example from a single subject). **A**) 3D reconstruction of ECoG channel locations from intraoperative CT. **B**) DBS lead location in the STN (marked with arrow) in an axial view of the preoperative MRI fused with the intraoperative CT. **C**) Placement of DBS lead (right) according to microelectrode map (left). Single units with 20–50 Hz irregular discharge, marked with dots, are used to define the borders of the STN. Cells that responded to passive arm or leg movements (red dots) localized the dorsal (motor) STN. **D**) Cortical evoked potentials in channels 1–14 elicited from ventral subthalamic stimulation (C0-C1+, 6 mA). Earliest latency potentials occur at ~2 ms. **E**) Ventral STN stimulation elicits larger

amplitude evoked potentials than dorsal STN stimulation. **F**) Cortical topography of evoked potential amplitudes in this subject. Amplitudes are higher over inferior frontal regions. **G**) Reversal of the stimulating anode and cathode reverses the polarity of the stimulation artifact (see inset), but not the polarity of the 2 ms potential, arguing against an artifactual origin of the 2 ms potential. See also Figure S1.

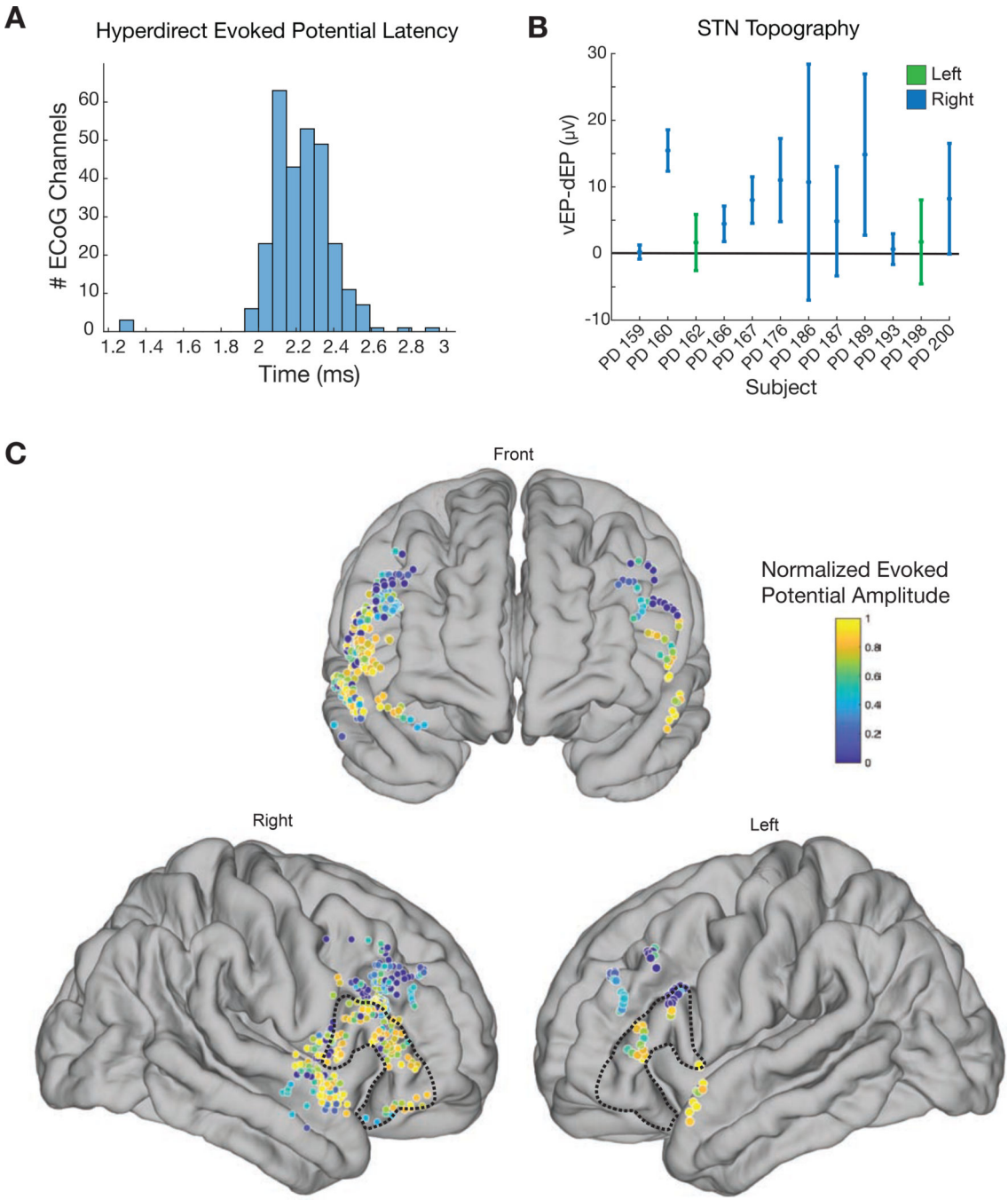

Figure 2.

Prefrontal cortical evoked potentials across all subjects show topography of the hyperdirect pathway. **A**) Histogram of latencies for the earliest evoked potential across all patients (mean 2.2 ± 0.2 ms). **B**) Larger potentials from ventral stimulation in most subjects. The mean and standard deviation of the difference between ventral versus dorsal evoked potential amplitudes are plotted for each subject. **C**) Composite 3D heatmap of the normalized evoked potential amplitudes. Color indicates the EP amplitude compared to the highest amplitude recorded in the same ECoG strip. The highest amplitudes are within the IFG regions (dotted

black line) or perisylvian temporal cortex in close proximity to IFG. Sulci appear larger in the atlas brain compared to an individual brain. See also Figures S1–S4.

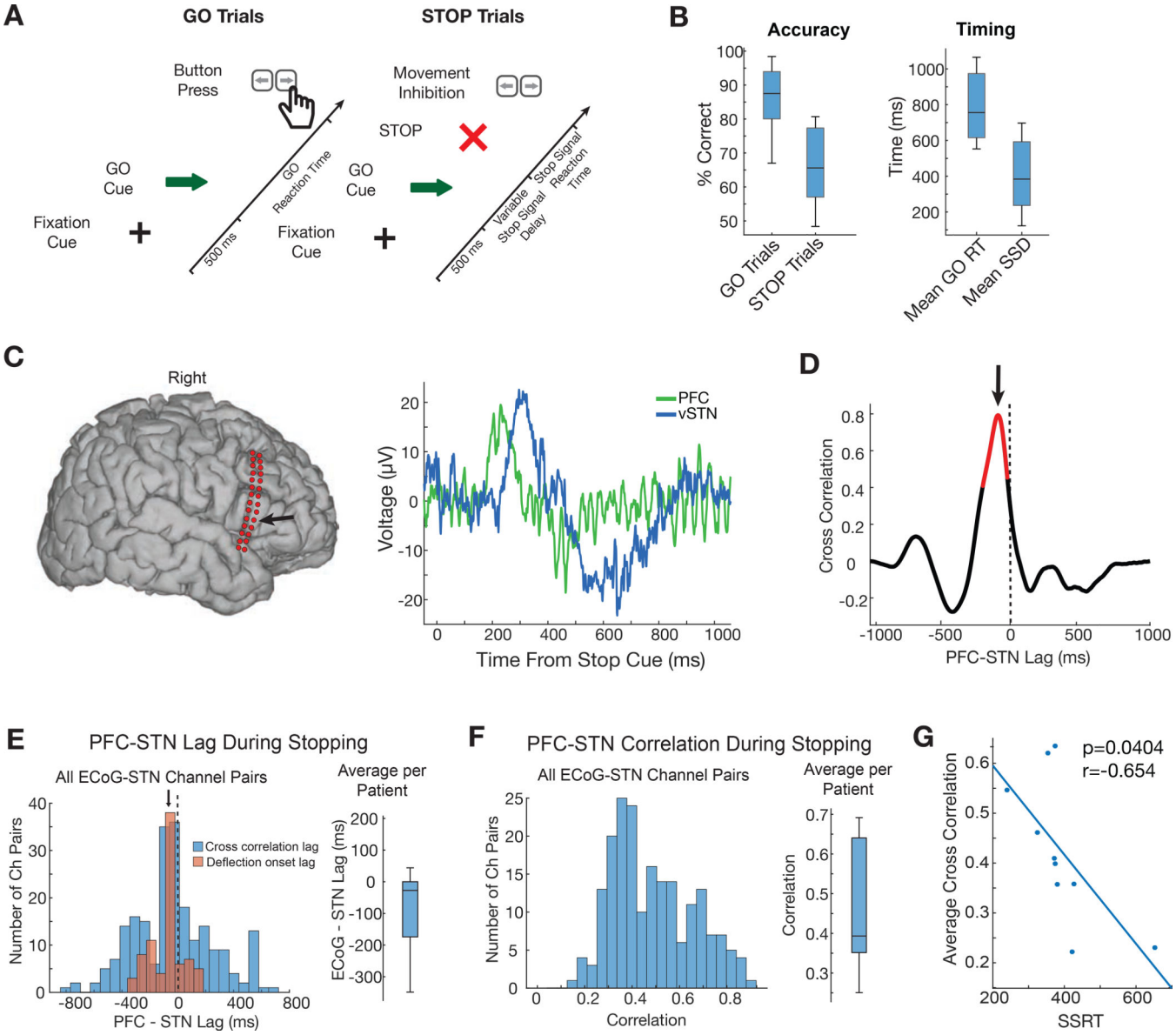

Figure 3.

Stopping-related potentials in the cortex and STN are correlated and their correlation predicts stop signal reaction time. **A**) Schematic of visual stop signal task. **B**) Behavioral performance on the task. **C**) Averaged event-related potentials of 41 successful stop trials time-locked to the stop cue in a single subject. Potentials were recorded from the ventral STN and from one cortical contact (location indicated with arrow on the brain reconstruction on the left). **D**) Cross correlation between cortical and subthalamic potentials for the subject in C. Red region indicates significant cross correlation. **E**) Cortico-subthalamic lag during stopping, calculated using two analytic methods, showing that prefrontal potentials precede those in the STN. Using cross correlation, the distribution of lags for all cortico-subthalamic channel pairs had a median lag of −71 ± 297 ms (blue). In channels with clear ERP deflection onset, we calculated the offset between ERP deflections, and the median lag was −61 ± 113 ms (red). Boxplot on the right shows the distribution of mean cross correlation

lags for each subject. **F**) Maximum correlation during stopping. All cortico-subthalamic channel pairs with significant cross correlation plotted in the left histogram, and boxplot on the right shows distribution of mean cross correlation values for each subject. **G**) The average cortico-subthalamic cross correlation during stopping is inversely correlated with estimated stop signal reaction time. See also Figure S5 and Figure S8.

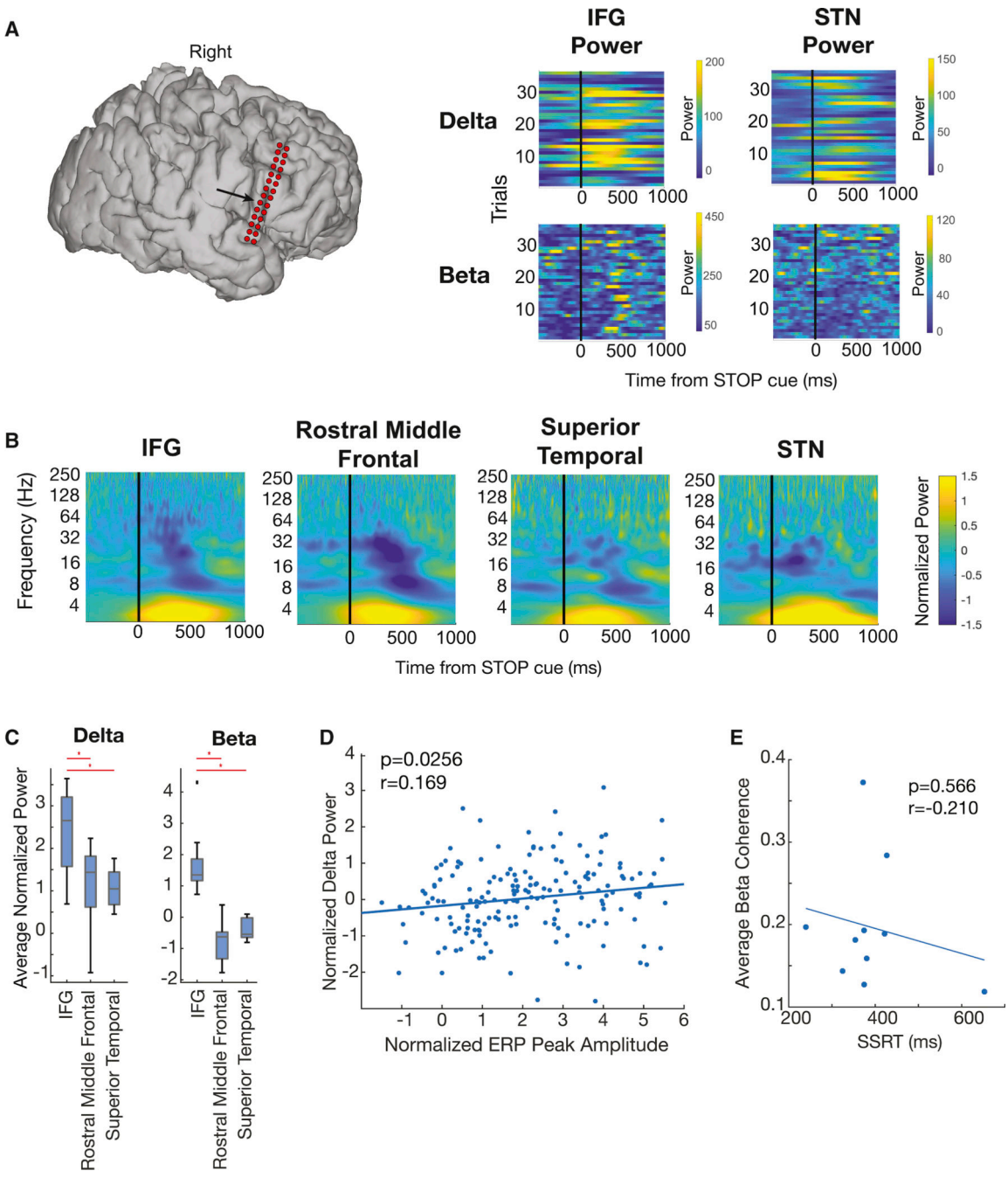

Figure 4.

Beta power is modulated during stopping, but IFG-STN beta coherence is not correlated with stopping behavior. **A**) In a single subject example, trial-by-trial modulation of delta (top) and beta (bottom) power during stopping, in the IFG (location indicated with arrow in brain reconstruction on the left) and STN. Trials are aligned to the STOP cue. **B**) Grand-averaged task-related spectrograms for all subjects. **C**) Quantification of task-related power modulation in the delta and beta frequencies for all subjects. Power in each frequency range was quantified in the 500 ms window surrounding each subject's stop signal reaction time. **D**) Correlation between stopping-related delta power and ERP peak amplitude for single

ECoG channels. Delta power and ERP peak amplitudes are z-score normalized per patient. **E**) Average stopping-related beta coherence (in 500 ms window surrounding stop signal reaction time) is not correlated with stop signal reaction time. See also Figure S6 and Figure S7.